Supporting information for:

New insights into the facilitated dissolution and sulfidation of silver nanoparticles under simulated sunlight irradiation in aquatic environments by extracellular polymeric substances

Yi Yang[a, 1], Shimei Zheng[b, 1], Ruixuan Li[a], Xin Chen[a], Kunkun Wang[a], Binbin Sun[a], Yinqing Zhang[a, *], Lingyan Zhu[a, *]

[a] Key Laboratory of Pollution Processes and Environmental Criteria (Ministry of Education), Tianjin Key Laboratory of Environmental Remediation and Pollution Control, College of Environmental Science and Engineering, Nankai University, Tianjin 300350, China

[b] College of Chemistry and Chemical and Environmental Engineering, Weifang University, Weifang 261061, China

[1] These authors contributed equally to this article.

Summary:

Number of pages: 31

Page S2-S10: Additional experimental details

Page S11-S13: Table S1-Table S3

Page S14-S29: Fig. S1–Fig. S16

Synthesis of the PVP-coated AgNPs.

AgNPs were synthesized following the method described by our previous study.[1] Briefly, 10 mL of 10 mM $AgNO_3$ was added into a 90 mL solution containing 1.67 mM hydroxylammonium chloride ($NH_2OH \cdot HCl$) and 3.31 mM sodium hydroxide (NaOH) under vigorous stirring. After several minutes, 0.30 g of PVP was introduced into the solution and stirred for the whole night. The products were collected by centrifugal ultrafiltration (Amicon Ultra-15 30 kDa, Millipore, USA) and purified with ultrapure water for three cycles. The stock suspension of AgNPs was stored at 4 °C in the dark for further experimental use.

Extraction and purification of EPS.

Chlorella vulgaris (FACHB-5) were grown in batch mode in BG11 medium under controlled ambient conditions at (25±1) ℃ and a 12 h light/ 12 h dark cycle with illumination of 4000 lux. EPS were extracted from algal solution according to the methods described by Chu *et al.* with slight modifications.[2] Briefly, when the cells reached the exponential growth phase, they were centrifuged at 4000 *g* for 10 min at 4 ℃ to remove medium. The pellets were washed with ultrapure water and resuspended to 50% of the original volume. To separate EPS form pure cells, the suspension was then centrifuged at 10800 *g* for 20 min at 4 ℃. The supernatant were collected and then filtered with 0.22 μm polyethersulfone (PES) membrane. The filtrate was then dialyzed against ultrapure water using regenerated cellulose tubular membrane of 3500 Da cut-off, which had been treated with $NaHCO_3$ and Na_2EDTA to remove residual salts from medium.[3] The dialyzed EPS were collected and stored at 4 ℃ in the dark for later analyses and experiments.

XPS analysis of EPS.

The functional groups were determined by X-ray photoelectron spectroscopy (XPS, Escalab 250Xi, Thermo Fisher Scientific, US) equipped with monochromatic Al Kα radiation source (1486.6 eV). The pass energies for elemental surface composition and chemical binding information of component speciation were 150 eV and 30 eV, respectively. The surface charging effects were calibrated using C 1s peak with a fixed binding energy of 284.8 eV.

The XPS spectra of EPS were shown in Fig. S3, and the binding energies were listed in Table S1. High resolution of C 1s, O 1s and N 1s XPS spectra were deconvoluted to assign appropriate functional groups. The C 1s peak around 284.80 eV was ascribed to C-(C, H) or aromatic C=C predominantly from polysaccharides or side chains of amino acids, and the peak around 286.36 eV was attributed to C-(O, N) from amine, alcohol, or amide groups in proteins. The weak peak around 287.66 eV was associated with C=O or O-C-O in carboxylate, carbonyl or amide in polysaccharides or proteins. Another weak peak around 288.68 eV was indicative of the presence of O=C-OH or O=C-OR in carboxyl or ester groups.[4-6]

Dissolved Ag^+ ions measurement.

Dissolved Ag^+ ions were separated from the suspensions by centrifugation at 5000 *g* for 20 min using ultrafiltration filters (Amicon Ultra-15 10 kDa, Millipore, USA). The concentration of dissolved Ag^+ ions was quantified to estimate the oxidative dissolution rate constant by inductively coupled plasma mass spectrometry (ICP-MS, 7700 ICP-MS system, Agilent, USA). AgNPs were not detected in the filtrate after centrifugation by UV-vis spectroscopy. These results indicated that the 10 kDa nominal weight cut-off was sufficient to separate AgNPs from dissolved Ag^+ ions. The recovery of the dissolved Ag was over 96% in the absence and presence of EPS, suggesting that adsorption to the filter was negligible.

Additional spectral analyses procedures.

A suite of spectroscopic analyses were applied to probe the interactions between EPS and AgNPs and the inherent mechanisms. The EPS (10 mg $C \cdot L^{-1}$) and AgNPs mixture solution were shaken on a thermostat shaker (200 rpm, 25 ℃) to achieve equilibrium. The residual EPS after the adsorption of AgNPs were obtained by centrifugation (8000 *g*, 15 min). The EPS solution initially and residual part were subjected to UV-vis absorption spectra scanning within the range of 200–800 nm. The values of specific ultraviolet absorbance (SUVA254) were calculated by dividing the absorbance at 254 nm with the TOC concentration.[7] The 3D-EEM of EPS in the absence and presence of AgNPs were obtained with subsequent scanning emission (Em) wavelength from 200 to 550 nm at 1 nm increment by varying the excitation (Ex) wavelength from 200 to 450 nm at 5 nm increments. Excitation and emission slits were set at 5 nm and the scanning speed was 1200 $nm \cdot min^{-1}$. The spectrum of ultrapure water was recorded as blank and each spectrum was the average of at least three scans. Each FTIR spectrum was obtained from 4000 to 650 cm^{-1} after an average of 32 scans with a spectral resolution of 4 cm^{-1}. ATR-FTIR spectra were processed by 2D-CoS analysis with 2D Shige software (Kwansei-Gakuin University, Japan). AgNPs concentration was used as the external perturbation to reveal the structural changes of EPS in the process of binding with AgNPs. The sequential orders were obtained from the auto-peaks and cross-peaks in the synchronous and asynchronous spectra of 2D-CoS. Corresponding details of 2D-CoS mathematical procedures can be found elsewhere[8] and are provided below as well. Then, the differences in the composition of secondary structures in EPS before and after the addition of AgNPs were determined. The amide I region (1700~1600 cm^{-1}), which is attributable to the C-O bond stretching vibrations of peptide groups in proteins, was further selected to extract information regarding the changes in the secondary structure of proteins. Specific

information can be found elsewhere[9, 10] and are descried below. The second derivative spectra of the original amide I were obtained using a nine-point Savitzky-Golay derivative function. The spectrum was deconvoluted to separate overlapping peaks based on the maximum absorption intensity, band frequency and bandwidth from the second derivative. A Lorentzian line shape was quantitated for the amide I region prior to curve fitting the original spectra using Peakfit 4.12 software.

Two-dimensional correlation spectroscopy (2D-CoS) analysis.

To obtain the structural variation information on the EPS-AgNPs interaction, 2D-CoS was employed using ATR-FTIR spectra with AgNPs concentration as the external perturbation. The 2D-CoS spectra were produced according to the method of Noda and Ozaki.[11] The involved algorithm adopted in the software has been summarized by Chen et al.[8] and is given below.

For the perturbation-induced spectral variation $Y(\lambda_i, C_k)$ as a function of a spectral variable (λ, the spectral wavelength of ATR-FTIR) and a perturbation variable (C, AgNPs concentration), a set of dynamic spectra $\tilde{Y}(\lambda_i, C_k)$ is defined as follows:

$$\tilde{Y}(\lambda_i, C_k) = \begin{cases} Y(\lambda_i, C_k) - \bar{Y}(\lambda_i), & 1 \le k \le m \\ 0, & otherwise \end{cases}$$

where $\bar{Y}(\lambda_i)$ denotes the reference spectrum, typically, the m variable-averaged spectrum.

$$\bar{Y}(\lambda_i) = \frac{1}{m}\sum_{k=1}^{m} Y(\lambda_i, C_k)$$

The synchronous (Φ) and asynchronous (Ψ) correlation spectra can be generated from the following transform:

$$\Phi(\lambda_1,\lambda_2) = \frac{1}{m-1}\sum_{k=1}^{m} \tilde{Y}(\lambda_1, C_k)\tilde{Y}(\lambda_2, C_k)$$

$$\Psi(\lambda_1,\lambda_2) = \frac{1}{m-1}\sum_{k=1}^{m} \tilde{Y}(\lambda_1, C_k)\sum_{k=1}^{m} N_{ik}\tilde{Y}(\lambda_2, C_k)$$

where the term Nik is the Hilbert-Noda transformation matrix defined as follows:

$$N_{ik} = \begin{cases} 0, & i = k \\ \dfrac{1}{\Pi(k-i)}, & otherwise \end{cases}$$

Synchronous correlation spectrum $\Phi(\lambda_1, \lambda_2)$ corresponding to the real part of the cross-correlation function represent the directionality of two spectral intensities measured at λ_1 and λ_2. If the sign of the cross-peaks $\Phi(\lambda_1, \lambda_2)$ is positive, the spectral intensities at λ_1 and λ_2 are either increasing or decreasing simultaneously. In reverse, if the direction is opposite, the sign of $\Phi(\lambda_1, \lambda_2)$ becomes

negative.

Asynchronous correlation spectrum $\Psi(\lambda_1, \lambda_2)$ reflects that the sequential order of intensity changes of two spectral intensities measured at λ_1 and λ_2 induced by the perturbation.

If the signs of $\Phi(\lambda_1, \lambda_2)$ and $\Psi(\lambda_1, \lambda_2)$ are same, variation in the spectral intensity at λ_1 always occurs prior to that at λ_2. The sequential order is reversed if $\Phi(\lambda_1, \lambda_2)$ and $\Psi(\lambda_1, \lambda_2)$ have the opposite signs. The variations at λ_1 and λ_2 are completely synchronized if $\Psi(\lambda_1, \lambda_2)$ is zero. If $\Phi(\lambda_1, \lambda_2) = 0$, the sequential order of intensity variations becomes indeterminate.

ROS measurements and quenching tests.

p-CBA (20 μM) and FFA (850 μM) were used as indicators for ·OH and $^1O_2$ in the irradiated EPS solution at preselected time, respectively. The concentrations of *p*-CBA and FFA were analyzed with a high-performance liquid chromatograph (HPLC, 1260, Agilent, USA) equipped with an Eclipse Plus−C18 column. The concentration of *p*-CBA was determined using a mobile phase of 65% methanol/ 35% water and a detection wavelength of 237 nm at a flow rate of 1 mL·min^{-1}. The loss of FFA was quantified using a mobile phase of 15% methanol/ 85% 0.1 wt% phosphoric acid and a detection wavelength of 235 nm at a flow rate of 1 mL·min^{-1}.[12, 13] After irradiation for predetermined intervals, 200 μL of the EPS solution was withdrawn and mixed with 10 μL 1 g·L^{-1} phenol red, 10 μL 0.5 mg·mL^{-1} HRP and 10 μL 0.77 M NaOH. The absorbance at 610 nm was measured to determine the generation of H_2O_2.[14] Measurements were performed in triplicate. To further investigate the roles of ROS in the dissolution of AgNPs, *tert*-butyl alcohol (TBA), furfuryl alcohol (FFA) and sodium pyruvate were introduced into the dissolution reaction system as scavengers of ·OH, $^1O_2$ and H_2O_2, respectively.[15, 16] Dissolution experiments of AgNPs were conducted with the addition of different scavengers at 200 μM in the presence of EPS (10 mg C·L^{-1}).

Table S1. Functional groups of EPS analyzed by high resolution XPS spectra in Fig. S3.

Region	Functional group	Binding energy (eV)	Atomic (%)
C 1s	C-(C, H), aromatic C=C	284.80	59.91
	C-(O, N)	286.36	23.27
	O-C-O, C=O	287.66	5.05
	O=C-OH, O=C-OR	288.68	9.81
O 1s	O=C	531.93	59.62
	C-O-C, C-O-H	532.94	40.38
N 1s	nonprotonated nitrogen	400.02	71.60
	protonated nitrogen	402.05	28.40

Table S2. 2D-IR-CoS results of the assignments and signs of cross-peaks in synchronous and asynchronous maps of EPS with increasing AgNPs concentration.

Wavenumber (cm^{-1})	Possible assignments in C-EPS	Ref.	Sign[a]				
			1045	1529	1550	1641	1708
1045	C-O-C, C-O and C-C in polysaccharides	[17]	+	(+,-)	(+,-)	(+,-)	(+,-)
1529	aromatic C=C stretching	[18]		+	(+,+)	(+,-)	(+,-)
1550	N-H stretching (amide II) in proteins	[18]			+	(+,-)	(+,-)
1641	C=O stretching (amide I) in proteins	[17]				+	(+,+)
1708	carboxylic acid C=O stretching vibration	[18]					+

[a]: Signs were obtained in the upper-left corner of the maps: +, positive; −, negative

Table S3. Variation of relative content of secondary structures in proteins of EPS for the interaction with AgNPs.

Secondary structures	Relative content (%)	
	EPS	EPS-AgNPs
aggregated strands	10.79	10.57
β-sheet	7.13	9.61
random coil	12.14	11.69
α-helix	25.82	27.19
3-turn helix	25.93	25.34
antiparallel β-sheet/aggregated strands	18.18	15.59

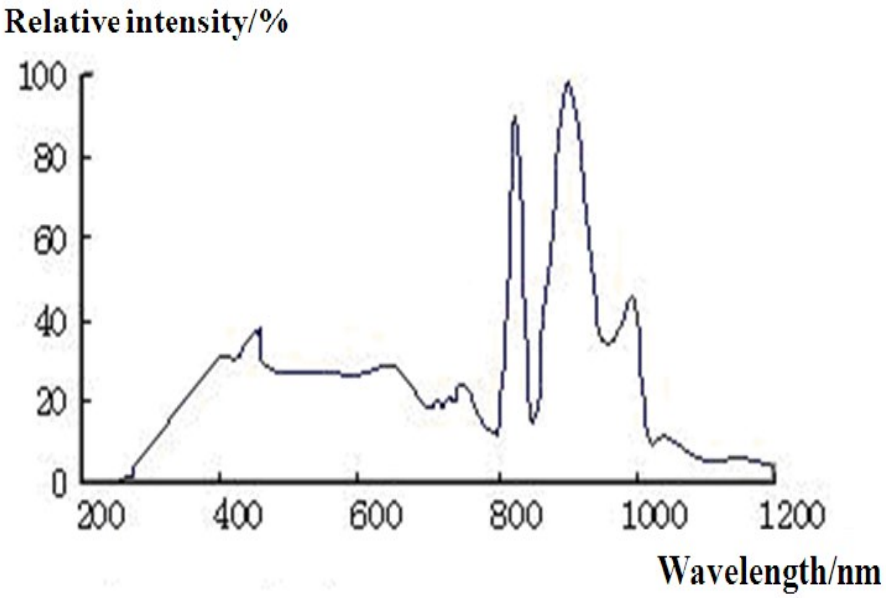

Fig. S1. The emission spectrum of the xenon lamp which was used to simulate sunlight irradiation.

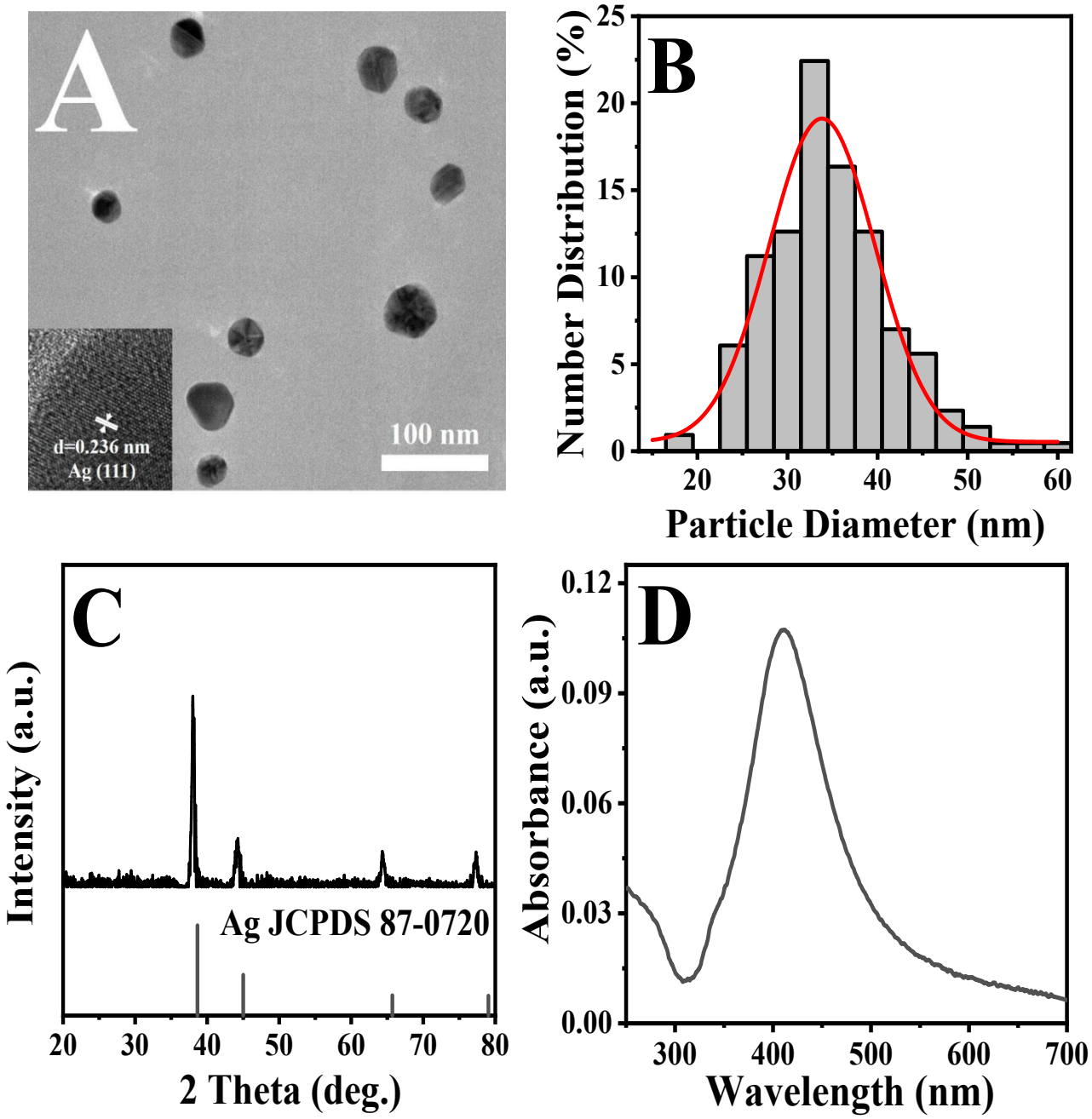

Fig. S2. Characterization of PVP-coated AgNPs. (A) A typical TEM image, (B) particle size distribution (counted more than 200 particles), (C) X-ray diffraction pattern, and (D) UV-vis spectra of freshly prepared AgNPs.

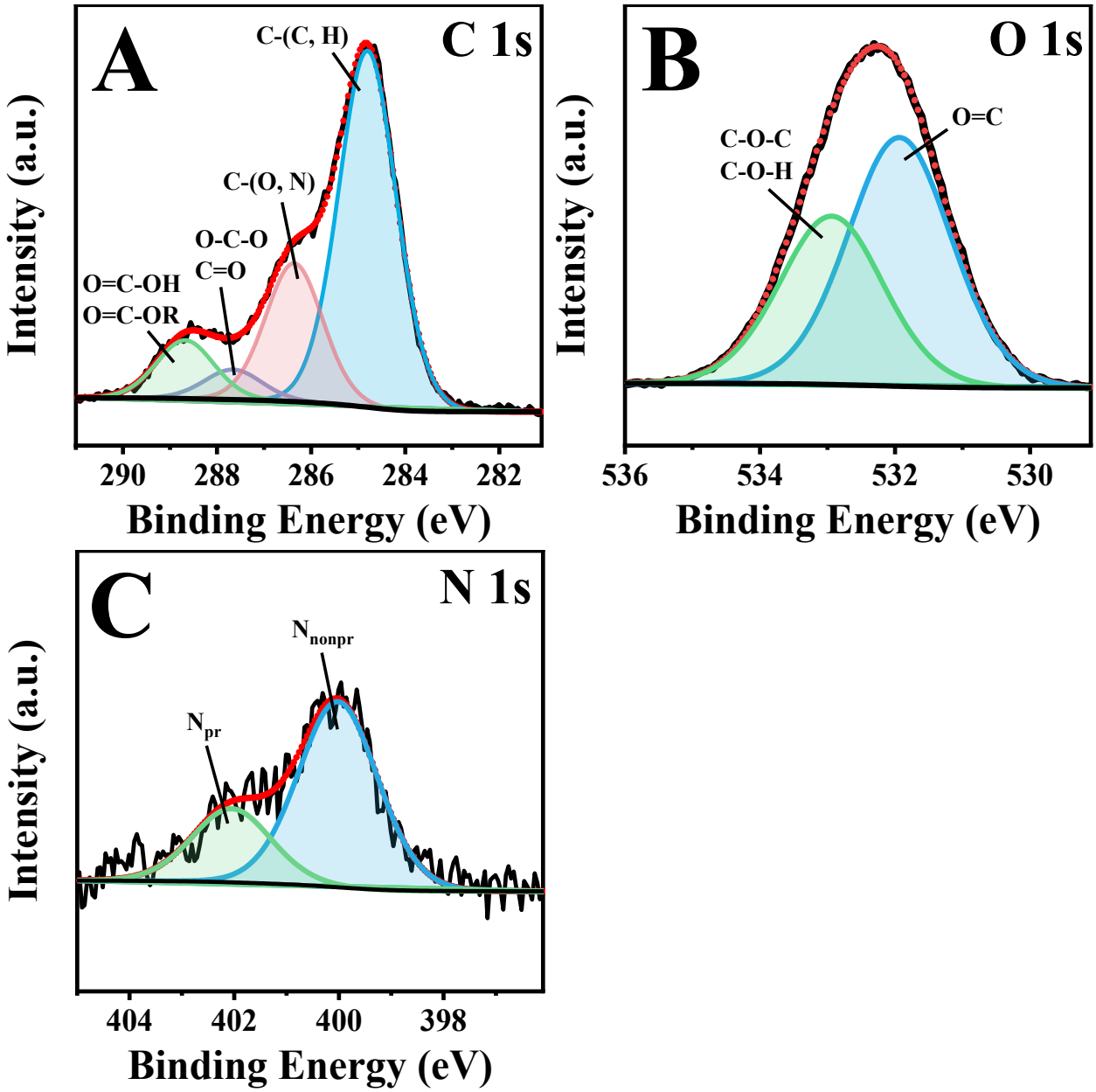

Fig. S3. High resolution of (A) C 1s, (B) O 1s and (C) N 1s XPS spectra of EPS.

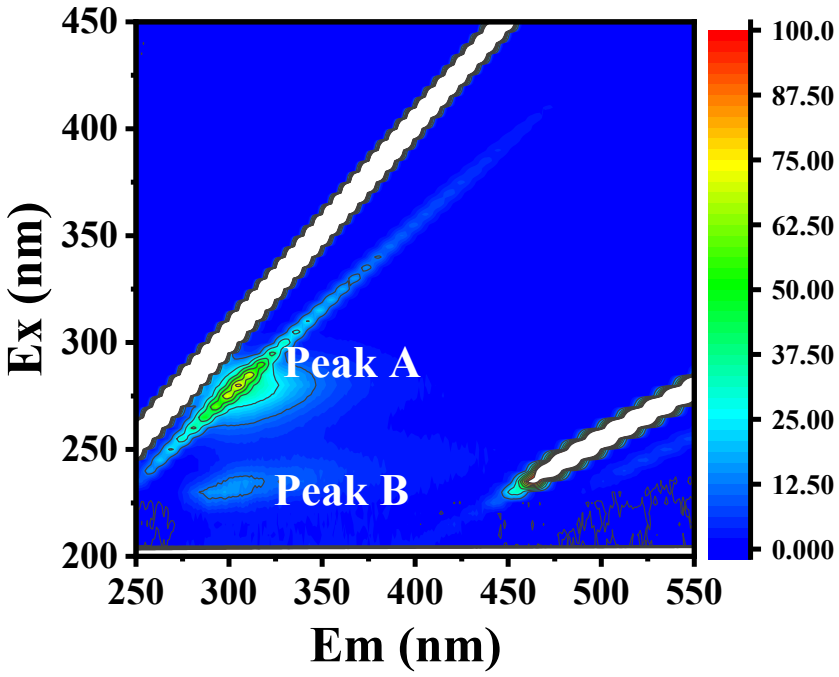

Fig. S4. Three-dimension excitation-emission matrix (3D-EEM) fluorescence spectra of EPS.

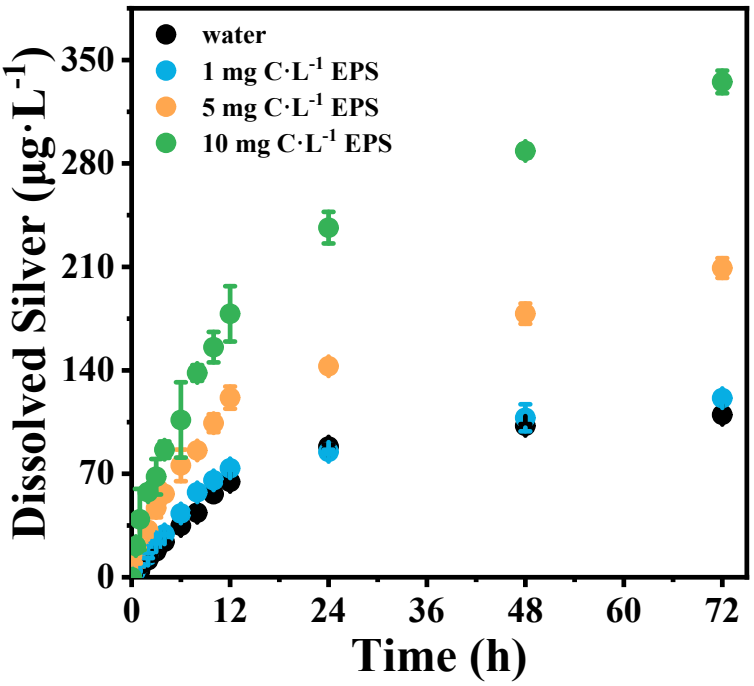

Fig. S5. Oxidative dissolution kinetics of AgNPs in the presence of EPS at different concentrations. Data points represent the average of three independent replicates.

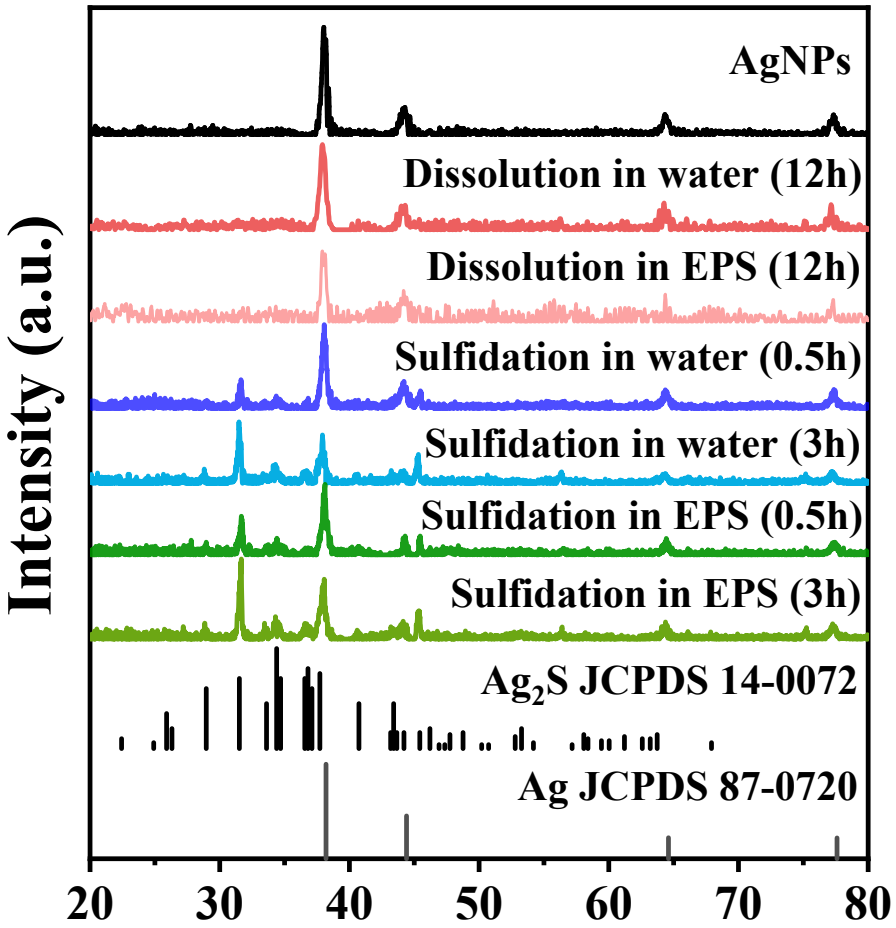

Fig. S6. XRD patterns of initial AgNPs, dissolution products after 12 h and sulfidation products at 0.5 h and 3 h in the absence and presence of EPS.

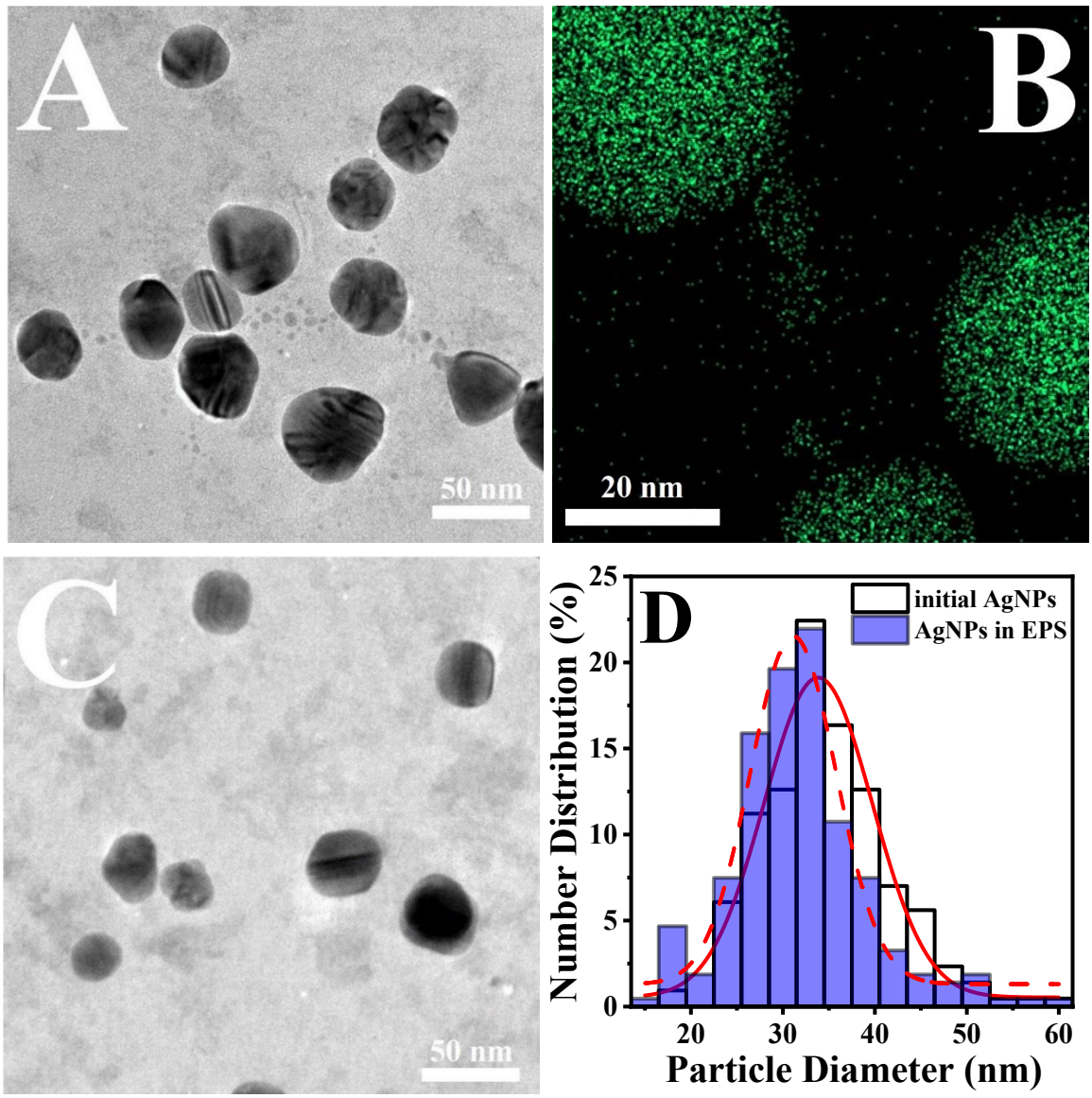

Fig. S7. (A) TEM images of AgNPs dispersed in 10 mg C·L^{-1} EPS suspension under irradiation for 1.5 h. The scale bar of the image represents 50 nm. (B) EDS elemental mapping analysis of Ag with green dots. The scale bar of the image represents 20 nm. (C) TEM images of AgNPs dispersed in 10 mg C·L^{-1} EPS suspension under irradiation for 10 h. The scale bar of the image represents 50 nm. (D) Particle size distribution of AgNPs initially and dispersed in EPS suspension under irradiation for 10 h. The counting number was more than 200 particles.

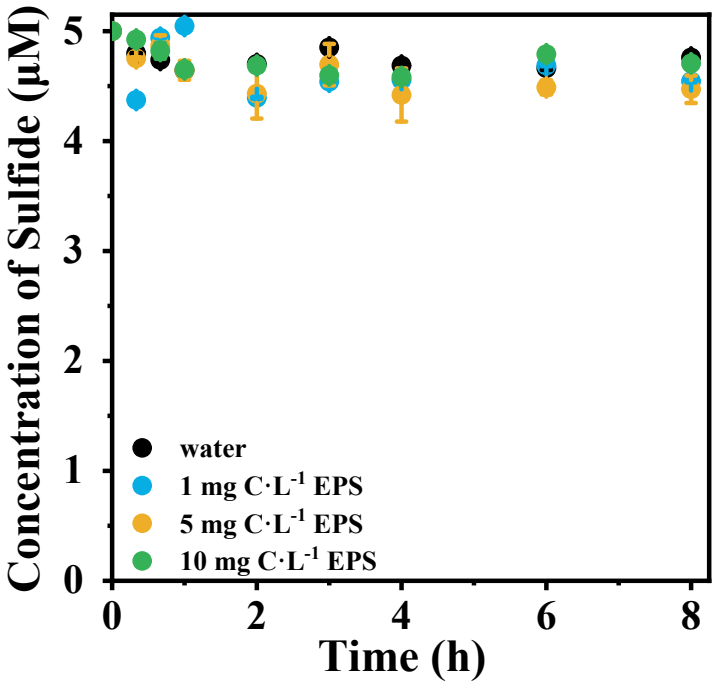

Fig. S8. Decrease of soluble sulfide concentration in EPS solution at different concentrations in the absence of AgNPs. Data points represent the average of more than three independent replicates.

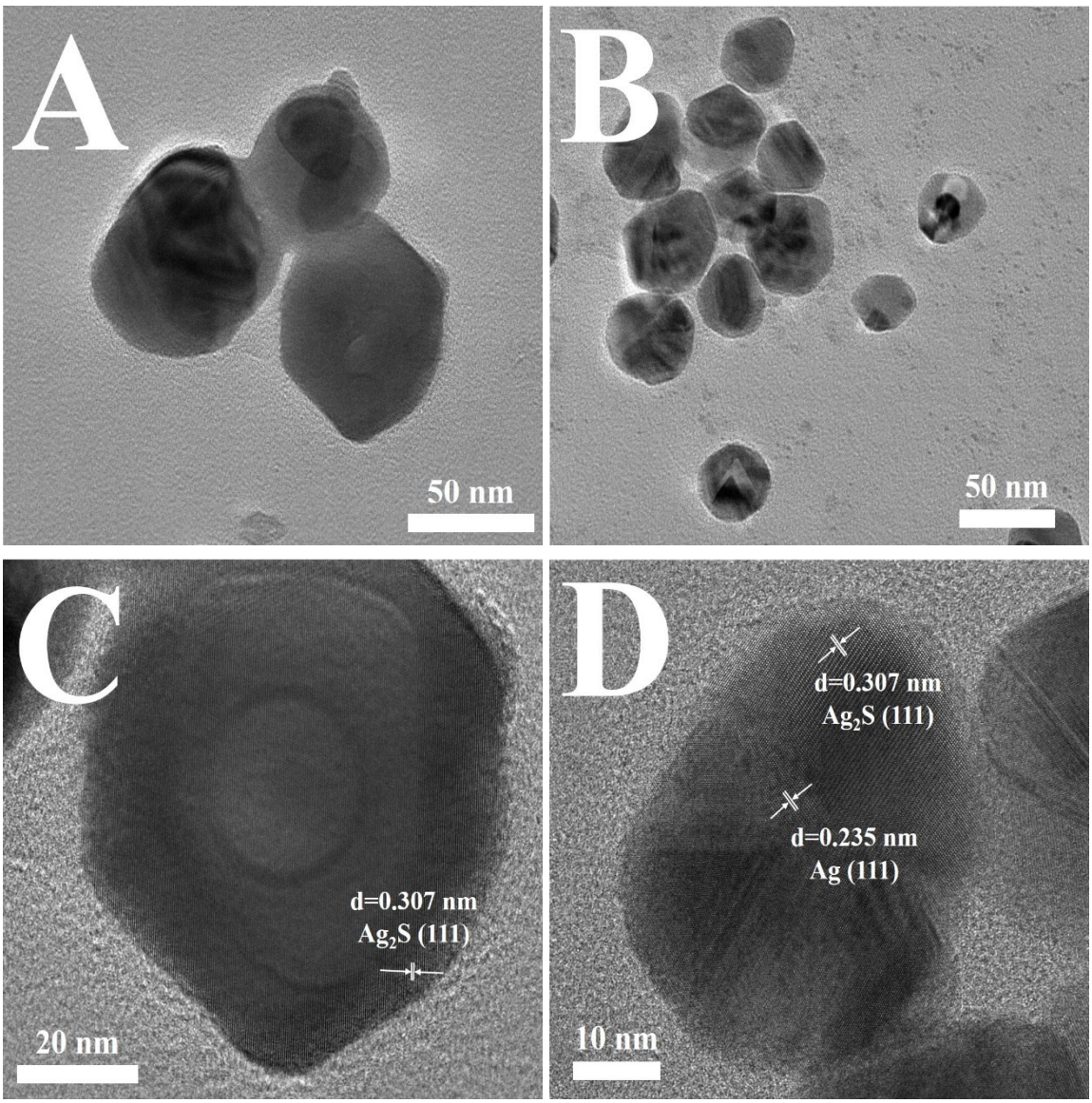

Fig. S9. TEM images of AgNPs sulfidation products in (A) water and (B) EPS solution. The corresponding HRTEM images of AgNPs sulfidation samples in (C) water and (D) EPS solution.

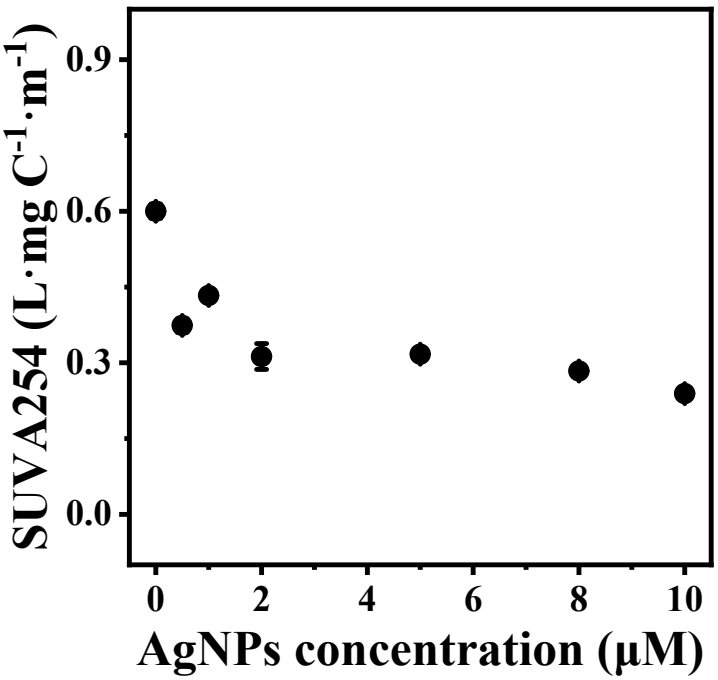

Fig. S10. The changes in SUVA254 obtained from the UV-vis spectra of the initial (10 mg C·L^{-1}) and residual EPS, which were collected by centrifugation after the adsorption equilibrium on AgNPs at different concentrations.

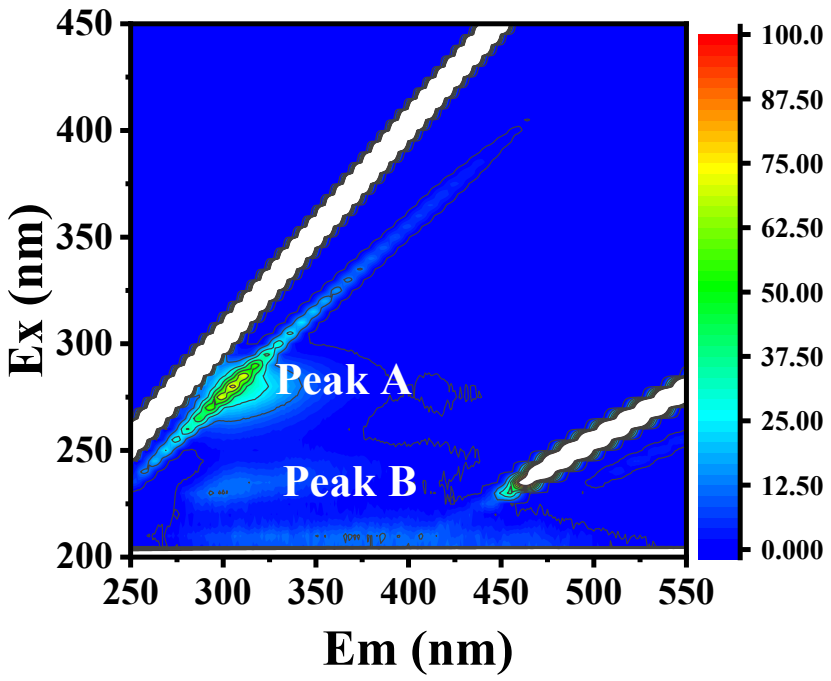

Fig. S11. Three-dimension excitation-emission matrix (3D-EEM) fluorescence spectra of EPS in the presence of AgNPs.

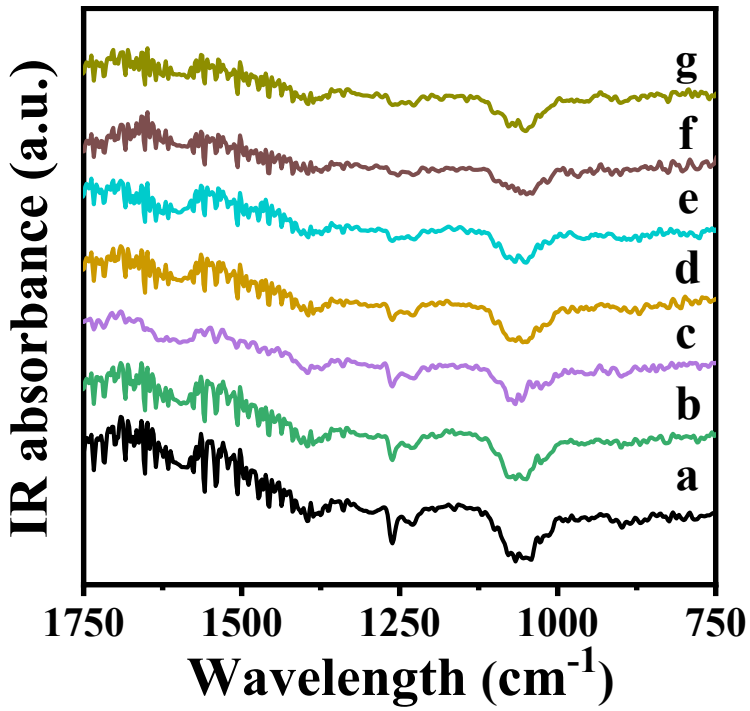

Fig. S12. Variations of ATR-FTIR absorption spectra of EPS after binding with AgNPs at increasing concentrations (a-g: 0, 0.5, 1, 2, 5, 8, 10 μM).

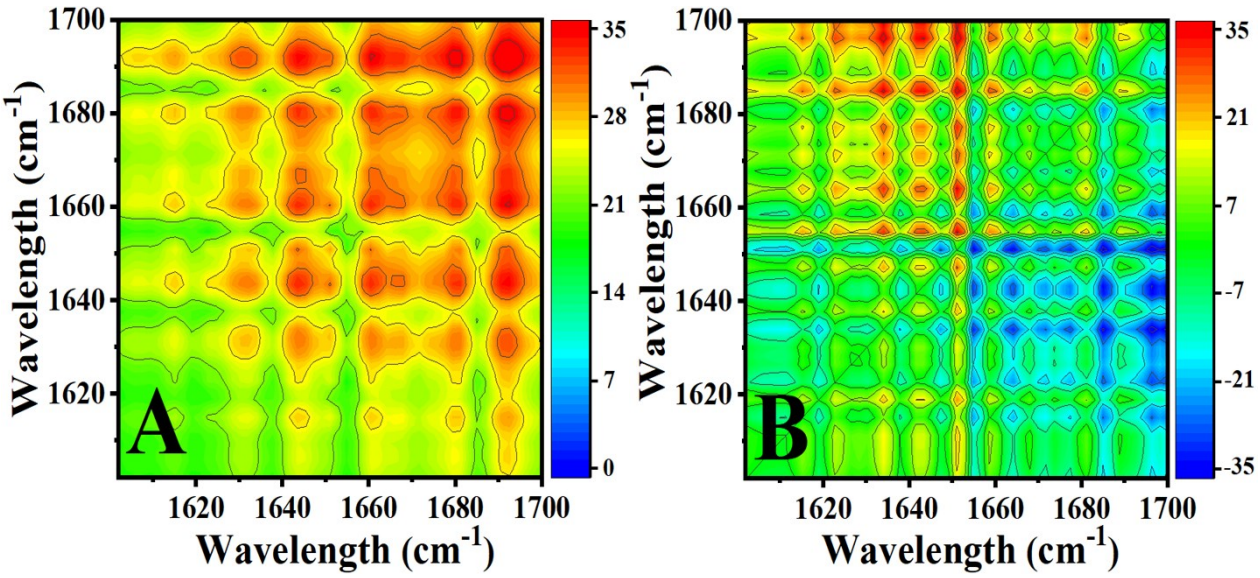

Fig. S13. (A) Synchronous and (B) asynchronous 2D correlation maps generated from the 1700-1600 cm^{-1} region of ATR-FTIR spectra of EPS with increasing AgNPs concentration.

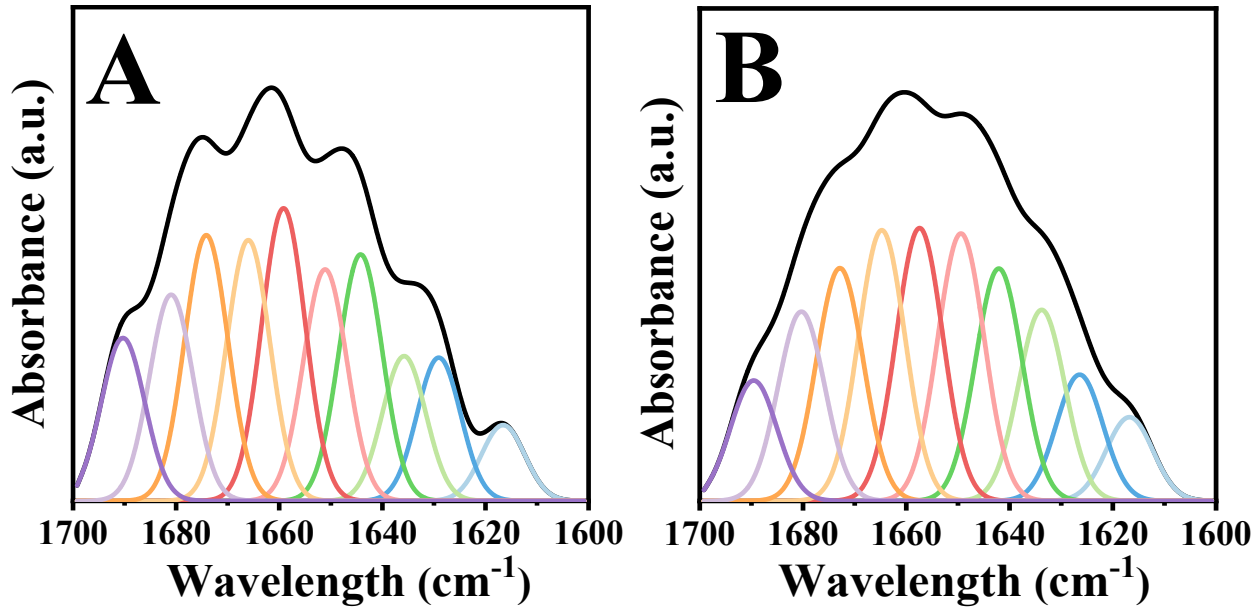

Fig. S14. Curve-fitted amide I region (1700-1600 cm^{-1}) for proteins of EPS in the (A) absence and (B) presence of AgNPs.

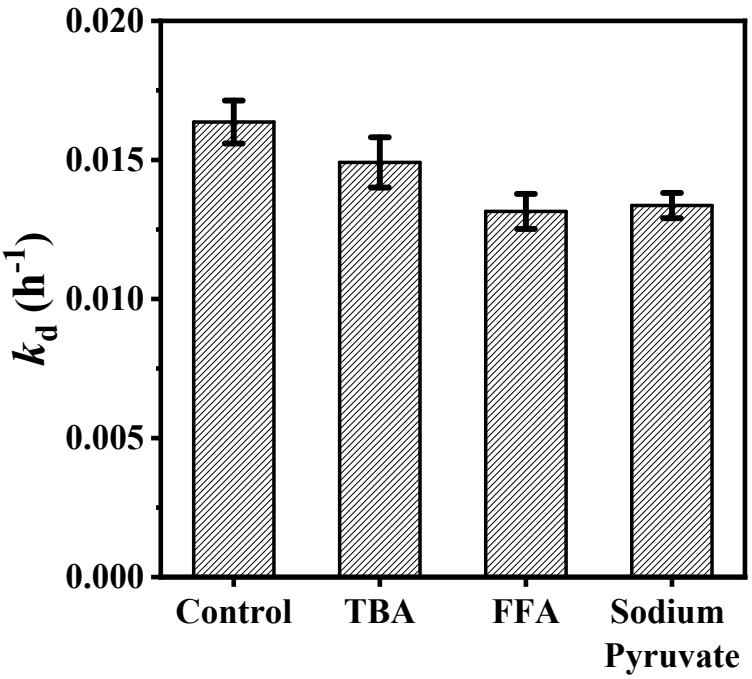

Fig. S15. The dissolution rate constants k_d of AgNPs with the addition of different scavengers in the presence of EPS (10 mg C·L^{-1}).

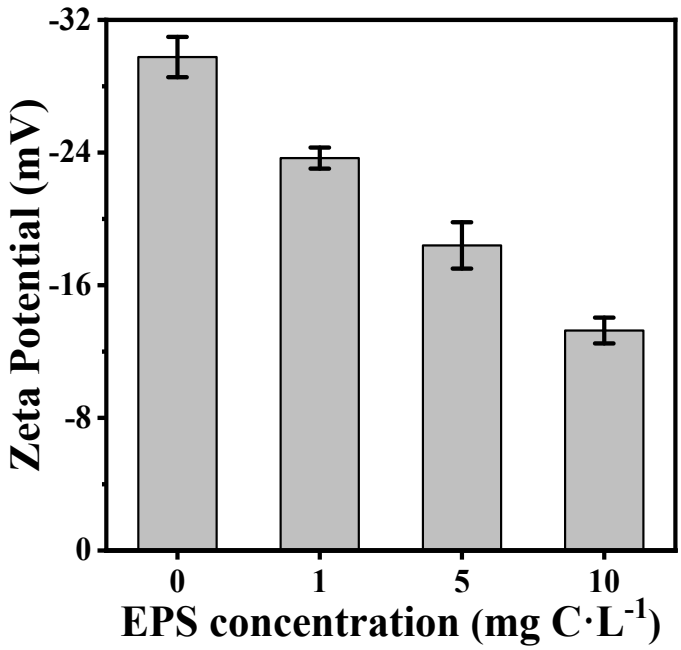

Fig. S16. Zeta potential of AgNPs before and after incubated in EPS solutions at different concentrations.

References

1. Y. Zhang, J. Xia, Y. Liu, L. Qiang and L. Zhu, Impacts of morphology, natural organic matter, cations, and ionic strength on sulfidation of silver nanowires, *Environ. Sci. Technol.*, 2016, **50**, 13283-13290.
2. H. Chu, H. Yu, X. Tan, Y. Zhang, X. Zhou, L. Yang and D. Li, Extraction procedure optimization and the characteristics of dissolved extracellular organic matter (dEOM) and bound extracellular organic matter (bEOM) from Chlorella pyrenoidosa, *Colloids Surf. B. Biointerfaces*, 2015, **125**, 238-246.
3. A. S. Adeleye, J. R. Conway, T. Perez, P. Rutten and A. A. Keller, Influence of extracellular polymeric substances on the long-term fate, dissolution, and speciation of copper-based nanoparticles, *Environ. Sci. Technol.*, 2014, **48**, 12561-12568.
4. Y. Liu, Z. Huang, J. Zhou, J. Tang, C. Yang, C. Chen, W. Huang and Z. Dang, Influence of environmental and biological macromolecules on aggregation kinetics of nanoplastics in aquatic systems, *Water Res.*, 2020, **186**, 116316.
5. C. S. He, R. R. Ding, J. Q. Chen, W. Q. Li, Q. Li and Y. Mu, Interactions between nanoscale zero valent iron and extracellular polymeric substances of anaerobic sludge, *Water Res.*, 2020, **178**, 115817.
6. Z. Zhang, R. Si, J. Lv, Y. Ji, W. Chen, W. Guan, Y. Cui and T. Zhang, Effects of extracellular polymeric substances on the formation and methylation of mercury sulfide nanoparticles, *Environ. Sci. Technol.*, 2020, **54**, 8061-8071.
7. W. Chen, P. Westerhoff, J. A. Leenheer and K. Booksh, Fluorescence excitation-emission matrix regional integration to quantify spectra for dissolved organic matter, *Environ. Sci. Technol.*, 2003, **37**, 5701-5710.
8. W. Chen, C. Y. Teng, C. Qian and H. Q. Yu, Characterizing properties and environmental behaviors of dissolved organic matter using two-dimensional correlation spectroscopic analysis, *Environ. Sci. Technol.*, 2019, **53**, 4683-4694.
9. L. J. Feng, J. J. Wang, S. C. Liu, X. D. Sun, X. Z. Yuan and S. G. Wang, Role of extracellular polymeric substances in the acute inhibition of activated sludge by polystyrene nanoparticles, *Environ. Pollut.*, 2018, **238**, 859-865.
10. C. Yin, F. Meng and G.-H. Chen, Spectroscopic characterization of extracellular polymeric substances from a mixed culture dominated by ammonia-oxidizing bacteria, *Water Res.*, 2015, **68**, 740-749.
11. I. Noda, Close-up view on the inner workings of two-dimensional correlation spectroscopy, *Vib. Spectrosc*, 2012, **60**, 146-153.
12. Y. Li, W. Zhang, J. Niu and Y. Chen, Surface-coating-dependent dissolution, aggregation, and reactive oxygen species (ROS) generation of silver nanoparticles under different irradiation conditions, *Environ. Sci. Technol.*, 2013, **47**, 10293-10301.
13. H. Liu, X. Gu, C. Wei, H. Fu, P. J. J. Alvarez, Q. Li, S. Zheng, X. Qu and D. Zhu, Threshold concentrations of silver ions exist for the sunlight-induced formation of silver nanoparticles in the presence of natural organic matter, *Environ. Sci. Technol.*, 2018, **52**, 4040-4050.
14. C. M. Wilke, B. Wunderlich, J.-F. Gaillard and K. A. Gray, Synergistic bacterial stress results from exposure to nano-Ag and nano-TiO2 mixtures under light in environmental media, *Environ. Sci. Technol.*, 2018, **52**, 3185-3194.
15. S. Zhu, X. Li, J. Kang, X. Duan and S. Wang, Persulfate Activation on Crystallographic Manganese Oxides: Mechanism of Singlet Oxygen Evolution for Nonradical Selective Degradation of Aqueous Contaminants, *Environ. Sci. Technol.*, 2019, **53**, 307-315.
16. M. Hopanna, L. Kelly and L. Blaney, Photochemistry of the Organoselenium Compound Ebselen: Direct Photolysis and Reaction with Active Intermediates of Conventional Reactive Species Sensitizers and Quenchers,

Environ. Sci. Technol., 2020, **54**, 11271-11281.

17. F. Kang, P. J. Alvarez and D. Zhu, Microbial extracellular polymeric substances reduce Ag+ to silver nanoparticles and antagonize bactericidal activity, *Environ. Sci. Technol.*, 2014, **48**, 316-322.
18. W. Chen, C. Qian, X. Y. Liu and H. Q. Yu, Two-dimensional correlation spectroscopic analysis on the interaction between humic acids and TiO2 nanoparticles, *Environ. Sci. Technol.*, 2014, **48**, 11119-11126.